

Accepted for the publication in the *Astrophysical Journal Letters*

A Half-Megasecond Chandra Observation of the Oxygen-Rich Supernova Remnant G292.0+1.8

Sangwook Park¹, John P. Hughes², Patrick O. Slane³, David N. Burrows¹, B. M. Gaensler⁴, and Parviz Ghavamian⁵

ABSTRACT

We report on our initial analysis of a deep 510 ks observation of the Galactic oxygen-rich supernova remnant (SNR) G292.0+1.8 with the *Chandra X-ray Observatory*. Our new *Chandra* ACIS-I observation has a larger field of view and an order of magnitude deeper exposure than the previous *Chandra* observation, which allows us to cover the entire SNR and to detect new metal-rich ejecta features. We find a highly non-uniform distribution of thermodynamic conditions of the X-ray emitting hot gas that correlates well with the optical [O III] emission, suggesting the possibility that the originating supernova explosion of G292.0+1.8 was itself asymmetric. We also reveal spectacular substructures of a torus, a jet, and an extended central compact nebula all associated with the embedded pulsar J1124–5916.

Subject headings: ISM: individual (G292.0+1.8) — supernova remnants — pulsars: individual (J1124–5916) — X-rays: ISM

1. INTRODUCTION

G292.0+1.8 is one of only three known “oxygen-rich” supernova remnants (SNRs) in the Galaxy (Goss et al. 1979; Murdin & Clark 1979), the others being Cassiopeia A and Puppis A. Optical emission from these SNRs contains fast-moving ($v \gtrsim 1000 \text{ km s}^{-1}$) O-rich ejecta knots, which

¹Department of Astronomy and Astrophysics, Pennsylvania State University, 525 Davey Laboratory, University Park, PA. 16802; park@astro.psu.edu

²Department of Physics and Astronomy, Rutgers University, 136 Frelinghuysen Road, Piscataway, NJ 08854-8019; also Department of Astrophysical Sciences, Princeton University, Peyton Hall, Princeton, NJ 08544-1001

³Harvard-Smithsonian Center for Astrophysics, 60 Garden Street, Cambridge, MA. 02138

⁴School of Physics, The University of Sydney, NSW 2006, Australia

⁵Department of Physics and Astronomy, Johns Hopkins University, 3400 North Charles Street, Baltimore, MD 21218

is generally taken as evidence for He-burning nucleosynthesis in the core of massive stars ($> 10 M_{\odot}$) (e.g., Blair et al. 2000). O-rich SNRs provide a rare opportunity for the study of core-collapse supernova (SN) nucleosynthesis and the subsequent evolution of the remnant, including in particular the interaction of ejecta fragments and the blast wave with circumstellar medium (CSM) produced by massive stellar winds from the progenitor. G292.0+1.8 is especially intriguing because it exhibits all the characteristics of a textbook-example core-collapse SNR: a central pulsar and pulsar wind nebula (PWN), metal-rich ejecta, shocked CSM, and the blast wave.

To facilitate a study of SNR G292.0+1.8 in unprecedented detail, we performed a deep AO7 *Chandra* observation during 2006 September 13–October 20, with the SNR centered on the I-array of the Advanced CCD Imaging Spectrometer (ACIS). Our ACIS-I observation takes advantage of a larger ($17' \times 17'$) field of view (FOV) and an order of magnitude deeper exposure (510 ks) than the previous *Chandra* ACIS-S3 observation ($8' \times 8'$ FOV and 43 ks exposure; Hughes et al. 2001). This new deep *Chandra* observation is an essential part of our multi-wavelength campaign on G292.0+1.8, including new observations in the radio, infrared, optical, and X-ray bands. Here we report on first results from the new *Chandra* images: a large-scale overview of the SNR in § 2 and new insights into the nature of the PWN in § 3. A description of the observations, data reduction, and results from extensive spectral and imaging analyses of detailed substructures of the SNR and PWN will be presented elsewhere.

2. Supernova Remnant

Figure 1 shows an X-ray color image of G292.0+1.8 created from our deep *Chandra* data. The outer boundary of the radio SNR is overlaid with a white contour. The energy bands displayed in each color were chosen to emphasize major atomic line emission that illustrates the distribution of electron temperatures and ionization states across the SNR (Table 1). We note that line and underlying continuum emission is included in each subband; e.g., the bright blue emission near the SNR’s center is dominated by synchrotron emission from the PWN (see the inset in Figure 1; Hughes et al. 2001). Our deep ACIS-I exposure comprehensively images the entire SNR to its faint outermost edge, which matches well the extent of the radio remnant (Figure 1) and traces the location of the blast wave. Ejecta knots (Park et al. 2004, Gonzalez & Safi-Harb 2003) appear brightly colored – yellow, green or blue – in Figure 1. They extend closest to the rim in the west and south and are furthest away in the SE quadrant. Due to their red-orange color in Figure 1 and positional coincidence with [O III] ejecta (Winkler & Long 2006), the southernmost X-ray knots are likely to be O-rich as well. The SNR’s full diameter is $\sim 9'.6$ (N-S) and $\sim 8'.4$ (E-W), corresponding to physical sizes of ~ 14.7 – $16.7 d_6$ pc, where d_6 is the distance to G292.0+1.8 in units of 6 kpc, the distance we assume throughout (Gaensler & Wallace 2003).

Our new image of G292.0+1.8 shows little evidence for the featureless, spectrally-hard, and geometrically-thin X-ray filaments that trace sites of efficient particle acceleration in other young SNRs, such as Cas A, Tycho, and SN 1006. Instead the SNR’s rim is defined by spectrally-soft

emission that is faint and diffuse in places (e.g., the SE rim) and filamentary elsewhere. Particle acceleration is evidently occurring under rather different conditions in G292.0+1.8 than other young Galactic SNRs.

The SNR interior contains a complex network of knots and filaments with a variety of colors and morphologies. The overall color distribution of these features is highly asymmetric; red-orange emission is dominant in the S-SE, while the W-NW regions are bright in emission appearing green-blue in color. We are confident that these variations largely reflect differences in the underlying distributions of gas temperature and ionization in the metal-rich ejecta, rather than variable foreground absorption. This is supported by the relative spatial distributions of the Ne He α and Ly α lines. Because these lines are separated in energy by only ~ 0.1 keV, their flux ratio is insensitive to absorption variations. The equivalent width maps show that Ne He α emission is relatively enhanced in the S-SE, while Ne Ly α emission is enhanced in the W-NW (Park et al. 2002). The metal abundance variation is also unlikely a significant contributor for the observed large-scale color variation based on our hardness ratio (HR) analysis (see below).

We constructed a HR map (Figure 2a) to investigate further the variation in the thermodynamic state of the ejecta across G292.0+1.8. (For technical reasons we added the continuum component [$E < 1.25$ keV] to the soft band line emission to enhance the hard band lines and suppress the strong hard continuum emission from the PWN.) There are prominent enhancements in Figure 2a near the W and NW boundary of the SNR that generally trace “fingers” of hot ejecta protruding out to the very boundary of the SNR (green-blue filaments in Figure 1). There is also an overall large-scale variation from HR values ~ 2.4 in the hard “NW” region to ~ 1.1 in the soft “SE” region (Figure 2a). Example spectra extracted from small regions within the larger “NW” and “SE” regions clearly show the distinctive line ratios responsible for the observed HR variation (Figure 2b). We can draw on our previous work fitting the spectra of individual knots to relate HR values to plasma temperatures. Spectral region 3 from Park et al. (2004) lies in the hard “NW” region, and spectral analysis yields a best-fit $kT \sim 5$ keV, corresponding to HR ~ 2.5 . We find that this HR value strongly traces the electron temperature rather than on individual elemental abundances. Although we did not study knots in the soft “SE” region previously, our preliminary spectral modeling of the SE regions favors significantly lower temperatures ($kT \sim 0.7$ keV), corresponding to HR values ~ 1.0 . Thus, the observed HR distribution reveals a large-scale spatial variation of thermal condition of metal-rich ejecta, which could not be detected by previous low-resolution data (Hughes & Singh 1994); i.e., a significantly higher temperature of the hot gas ($kT \sim 5$ keV) is implied in the N-W regions, while a relatively lower-temperature plasma ($kT \lesssim 1$ keV) prevails in the S-E regions of the SNR.

There is also a very similar and highly significant gradient in the optical properties of G292.0+1.8. The region with the lowest HR values is coincident with the bulk of the optical [O III] emission indicated by “SE” region in Figure 2a (Ghavamian et al. 2005; Winkler & Long 2006). Across the projected middle of the SNR (within an $\sim 3'$ wide region aligned roughly N-S), there are dozens of isolated optical knots (generally uncorrelated with X-ray knots), while on the western edge no opti-

cal emission appears at all. This high degree of correlation between the optical and X-ray properties suggests the possibility that radiative cooling in the ejecta is responsible for the SE-NW gradient in observed properties. In this picture, the SE ejecta would be undergoing significant, perhaps catastrophic cooling. Across the projected middle of the SNR, cooling is probably just beginning to occur in isolated knots that happen to have the appropriate thermodynamic conditions, while the emission toward the NW remains fully nonradiative. Variation in the ambient density surrounding G292.0+1.8 could provide an explanation for the observed asymmetry in the ejecta properties. However, there is no evidence for a higher density in the SE regions (Braun et al. 1986) as would be expected. In fact, 60 μm images¹ (see upper right and upper left insets to Figure 1) show that around the rim of the SNR the SE region is a minimum in flux, while the SW is a maximum. Thus, albeit somewhat speculative at the current stage of the analysis, we raise the possibility that the ejecta asymmetry has its origin in some intrinsic asymmetry of the SN explosion itself, such as a variation in the density or velocity distribution from SE to NW. Further work including detailed X-ray spectral analysis of ejecta and hydrodynamic studies appropriate for G292.0+1.8 are required to test this asymmetric explosion scenario.

3. Pulsar Wind Nebula

Previous *Chandra* observations of G292.0+1.8 (Hughes et al. 2001) revealed a point source, now known to be the pulsar J1124–5916 (Camilo et al. 2002; Hughes et al. 2003), powering an extended synchrotron nebula (Torii et al. 1998) (see the lower left inset to Figure 1). The emission from the pulsar itself was observed to be surrounded by a compact elliptical structure roughly $1''.8 \times 1''$ in size. Our deep ACIS-I observation confirms this structure, and reveals additional faint emission suggestive of a jet/torus structure ($\sim 5''$ in jet length and torus radius, respectively; see the lower right inset to Figure 1) similar to those observed to form just outside the pulsar wind termination shock region in a number of other young PWNe (e.g., Gaensler & Slane 2006 and references therein). Our preliminary spectral analysis indicates that these features show a power law spectrum with photon index $\Gamma \sim 1.5\text{--}1.8$, supporting the idea that they are synchrotron emission associated with the PWN. The ratio between the N-S and E-W sizes of the torus implies an inclination of the axis of the torus (with respect to the line of sight) of $\sim 20^\circ$. Physical sizes are then $\sim 0.4 d_6$ pc for the jet and a radius of $\sim 0.15 d_6$ pc for the torus. This is similar to the size of the jet/torus structure observed in 3C 58 (Slane et al. 2002), although we note that there is large

¹The apparent differences in the detailed structure of the two IR images in Figure 1 are unlikely to be real because of the highly processed nature of both images. The *ISO* image was constructed from a raster scan of many pointings using a 3×3 pixel ($\sim 45''$ per pixel) IR array that, unfortunately, did not fully cover the SE rim of the SNR. The *IRAS* image, which did cover the entire SNR, was the result of an image reconstruction process intended to improve the angular resolution from the native value of several arcminutes to the level of $1'\text{--}2'$. Given these significant differences, the overall general agreement between the images, specifically, the brightness of the SW rim and the faintness toward the SE, seems reasonable to us.

variation in the size and relative brightness of such structures from system to system.

Since the E-W “belt” of the SNR (Tuohy et al. 1982) appears to be a relic feature of the progenitor star’s equatorial winds (Park et al. 2002), the pulsar spin-axis defined by the N-S orientation of the jet is generally aligned with the progenitor’s rotation axis, at least in projection. If the pulsar position offset to the SE of the radio center of the SNR represents the direction of the pulsar velocity, a misalignment of $\theta \sim 70^\circ$ between the projected velocity and spin-axis vectors is implied.

This is in contrast to the strong tendency toward spin-kick alignment claimed by Ng & Romani (2007), although it is important to note that many of their estimated velocity vectors are, like ours, based on pulsar offsets from the geometric centers of their host SNRs – a technique that is quite sensitive to the ambient density since the SNRs will expand more rapidly in the direction of lower density, thus creating a shell that is not centered on the explosion point. Without a proper motion measurement, our results for J1124–5916 are thus not conclusive, although the density distribution inferred from the 60 μm data, which is enhanced in the NW-W-SW direction, is difficult to reconcile with the current pulsar position if the observed spin axis is aligned with the velocity vector. Finally, we note that our results are even consistent with possible orthogonality between the spin and kick directions, as might be suggested for some pulsars based on polarization measurements (Johnston et al. 2005; Rankin 2007).

4. Summary

Our deep *Chandra* observation of SNR G292.0+1.8 detects the entire outer boundary of the blast wave and reveals metal-rich ejecta knots reaching the shock front. We find no evidence for strong particle acceleration sites in X-rays. The initial large-scale analysis reveals a highly non-uniform distribution of X-ray emitting hot gas. This overall structure is caused by an asymmetric distribution of the gas temperatures, rather than variable foreground absorption. The expected properties of the ambient medium required to explain this asymmetry are inconsistent with observations, which leads us to the supposition that the supernova explosion itself was asymmetric. A detailed X-ray spectral analysis of the metal-rich ejecta and hydrodynamical simulations will be required to test this scenario. Proper motion measurements of the blast wave using the new radio data and detailed IR/optical studies of thermal states of cooling ejecta will also be important tests.

We discover a torus and a jet associated with the PWN of the embedded pulsar J1124–5916, similar to a growing number of such structures observed in other young pulsar-driven systems. Assuming that the pulsar’s birthplace was at the geometric center of the radio SNR and that the jet defines the direction of the pulsar spin axis, we find a large misalignment of $\sim 70^\circ$ between the spin and kick velocity directions, in apparent contrast to suggestions of spin-kick alignments in other systems.

The authors thank the *Chandra* Education and Public Outreach group for their help to generate the X-ray color image. This work was supported in part by Smithsonian Astrophysical Observatory under *Chandra* grant GO6-7049A (Penn State), GO6-7049B (Johns Hopkins), and GO6-7049C (Rutgers). P.G. was also supported by *Hubble Space Telescope* grant HST-GO-10916.06-A.

REFERENCES

- Blair, W. P. et al. 2000, *ApJ*, 537, 667
- Braun, R., Goss, W. M., Caswell, J. L., & Roger, R. S. 1986, *A&A*, 162, 259
- Camilo, F., Manchester, R. N., Gaensler, B. M., Lorimer, D. R., & Sarkissian, J. 2002, *ApJ*, 567, L71
- Cao, Y., Terebey, S., Prince, T. A., & Beichman, C. A. 1997, *ApJS*, 111, 387
- Gaensler, B. M. & Wallace, B. J. 2003, *ApJ*, 594, 326
- Gaensler, B. M. & Slane, P. O. 2006, *ARAA*, 44, 17
- Ghavamian, P., Hughes, J. P. & Williams, T. B. 2005, *ApJ*, 635, 365
- Gonzalez, M. & Safi-Harb, S. 2003, *ApJ*, 583, L91
- Goss, W. M., Shaver, P. A., Zealey, W. J., Murdin, P., & Clark, D. H. 1979, *MNRAS*, 188, 357
- Hughes, J. P. & Singh, K. P. 1994, *ApJ*, 422, 126
- Hughes, J. P., Slane, P. O., Burrows, D. N., Garmire, G. P., Nousek, J. A., Olbert, C. M., & Keohane, J. W. 2001, *ApJ*, 559, L153
- Hughes, J. P., Slane, P. O., Park, S., Roming, P. W. A., & Burrows, D. N. 2003, *ApJ*, 591, L139
- Johnston, S., Hobbs, G., Vigeland, S., Kramer, M., Weisberg, J. M., & Lyne, G. 2005, *MNRAS*, 364, 1397
- Murdin, P., & Clark, D. H. 1979, *MNRAS*, 189, 501
- Ng, C.-Y. & Romani, R. W. 2007, *ApJ*, 660, 1357
- Park, S., Roming, P. W. A., Hughes, J. P., Slane, P. O., Burrows, D. N., Garmire, G. P., & Nousek, J. A. 2002, *ApJ*, 564, L39
- Park, S., Hughes, J. P., Slane, P. O., Burrows, D. N., Roming, P. W. A., Nousek, J. A., & Garmire, G. P. 2004, *ApJ*, 602, L33
- Rankin, J. M. 2007, *ApJ*, 664, 447

Slane, P. O., Helfand, D. J., & Murray, S. S. 2002, *ApJ*, 571, L45

Torii, K., Tsunemi, H., & Slane, P. O. 1998, in *The Hot Universe*, Proc. of IAU Symp. No. 188, eds. K. Koyama, S. Kitamoto, & M. Itoh, (Dordrecht:Kluwer Academic), 258

Tuohy, I. R., Clark, D. H., & Burton, W. M. 1982, *ApJ*, 260, L65

Winkler, P. F. & Long, K. S. 2006, *AJ*, 132, 360

Table 1. Energy Bands Used to Generate the X-ray Color and Hardness Ratio Images.

Energy Band (keV)	Identification	Color	Energy Band (keV)	Identification	Color
0.40–0.50	Continuum	-	1.16–1.25	Continuum	-
0.58–0.71	O Ly α	Red	1.28–1.43	Mg He α	Green
0.75–0.84	Continuum	-	1.81–2.05	Si He α	Blue
0.88–0.95	Ne He α	Red	2.40–2.62	S He α	Blue
0.98–1.10	Ne Ly α	Orange	-	-	-

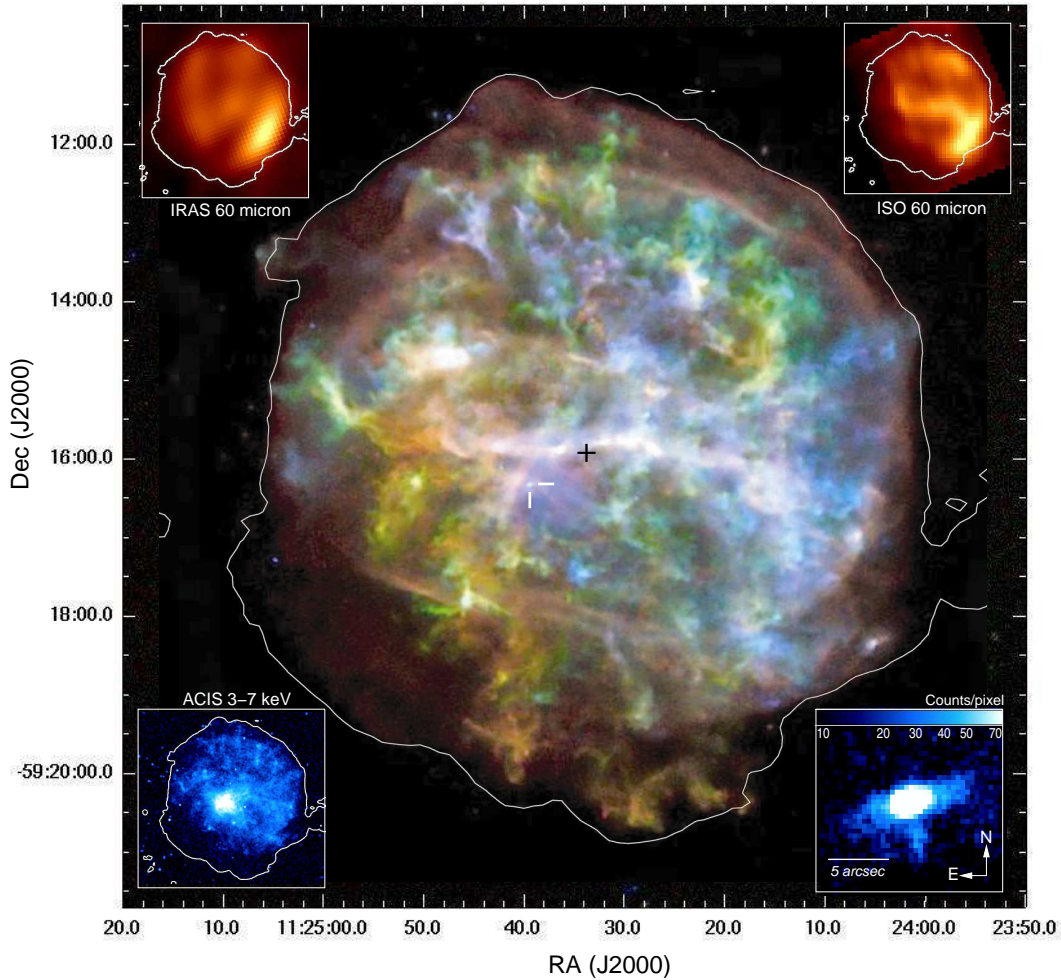


Fig. 1.— An X-ray-color image of G292.0+1.8. Red is the sum of the 0.58–0.71 and 0.88–0.95 keV bands (dominated by emission from O Ly α and Ne He α), orange is the 0.98–1.10 keV band (Ne Ly α), green is the 1.28–1.43 keV band (Mg He α), and blue is the sum of the 1.81–2.05 and 2.40–2.62 keV bands (Si He α + S He α). Each subband image has been exposure-corrected, binned with 2×2 pixels ($\sim 1''$), and smoothed for the purposes of display. The radio SNR center (Gaensler & Wallace 2003) is marked with a black cross. The position of PSR J1124–5916 (Hughes et al. 2003) is marked with white bars near the SNR center. *Lower left* inset is the 3–7 keV band image (binned by 4×4 pixel and smoothed by a Gaussian with $\sigma = 2$ pixels). The brightest central parts of the PWN is saturated to white. *Lower right* inset is the 2–7 keV band image of the PWN ($20'' \times 20''$ FOV centered on the pulsar position). The image is unbinned ($0''.492$) and smoothed by a Gaussian with $\sigma = 1$ pixel to emphasize the faint torus and jet. *Upper left* and *upper right* insets are the 60 μm images from *IRAS* Galaxy Atlas (Cao et al. 1997) and archival *ISO* data, respectively. In all panels except for the *lower right*, a boundary contour from the 20 cm radio image taken by Australian Telescope Compact Array is overlaid.

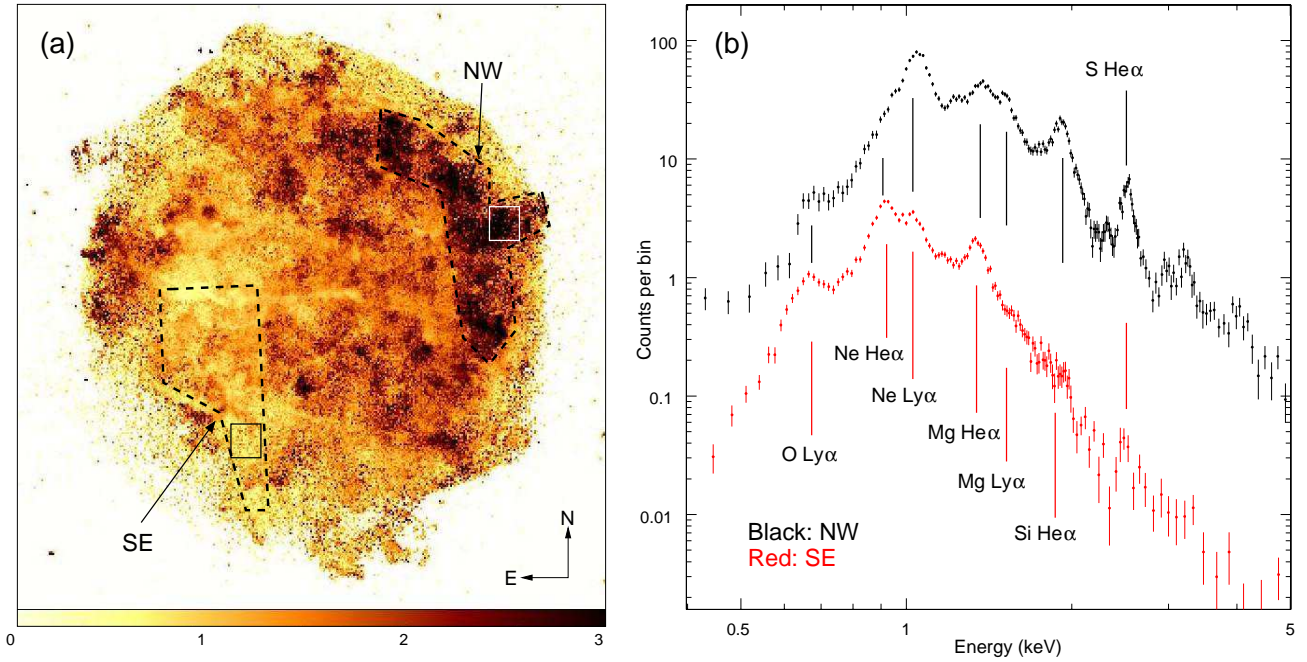


Fig. 2.— (a) A hardness ratio map of G292.0+1.8: $HR = (Ne\ Ly\alpha + Mg + Si + S) / (O + Ne\ He\alpha + \text{continuum}[E < 1.25\ keV])$. Energy bands used for line and continuum images are presented in Table 1. Each subband image has been binned with 4×4 pixels. (b) Example spectra representing “NW” (black) and “SE” (red) regions. Each spectrum has been arbitrarily scaled for the purposes of display. In (a), the small region where each spectrum was extracted is marked with a solid box. Regions outlined by the dashed polygon correspond to the location of bright diffuse [O III] emission (“SE” region), and the highest HR (“NW” region).